Evaluation of the GHBMC Lumbar Spine in Sub-injurious and Injurious Loading

Sophia K. Tushak, Bronislaw D. Gepner, Bengt Pipkorn, Jason R. Kerrigan

Abstract Accurate prediction of lumbar spine response and how it relates to kinematics, kinetics, and injury is critical since lumbar spine loading is predicted to be amplified in reclined postures. The objective was to evaluate the Global Human Body Models Consortium (GHBMC) lumbar spine (v5.1.1) model relative to post-mortem human subjects (PMHS) in two different loading modes using data from recent experiments. The model's whole ligamentous lumbar spine was first evaluated in sub-injurious quasi-static loading in multiple directions with three different levels of axial compression. Compared to PMHS, the GHBMC responses varied widely across loading direction and axial compression level, exhibiting higher stiffness in some conditions and lower stiffness in other conditions. Then, three-vertebra sections of the model's ligamentous lumbar spine were subjected to high-rate compression-flexion loading to failure. Compared to PMHS, GHBMC responses and stiffness coefficients did not display the same bilinear response behavior, but instead displayed linear behavior. Additionally, the GHBMC and PMHS did not respond similarly when increased levels of axial compression were applied. The outcomes from this study shed light on the usefulness of the model.

Keywords human body model, lumbar spine, GHBMC, kinetic response, kinematic response, stiffness

I. INTRODUCTION

The usage of human surrogates is fundamental in the field of injury biomechanics. Among the most frequently used are post-mortem human subjects (PMHS), anthropomorphic test devices (ATDs), and human body models (HBMs). Specifically, HBMs are computationally efficient, reproducible, and repeatable, and their usage continues to increase in the industry and academia. However, HBMs must be validated against existing experimental data to prove that their response to loading is similar to their experimental counterparts and accurately mimics human response, or is biofidelic. HBMs, such as the Global Human Body Model Consortium (GHBMC) and Total HUman Model for Safety (THUMS), are among the most evaluated and widely used. These HBMs have been validated against experimental data on the component level and whole-body level, and continue to be validated with the introduction of new experimental data for different body regions and loading scenarios as they become available.

Injury to the lumbar spine in motor vehicle crashes (MVCs) has become a topic of increased research efforts in the past several years, primarily due to the potential introduction of autonomous driving systems in which occupants may be able to recline further back in the seat. In a reclined posture compared to an upright posture, at the onset of a frontal MVC, the horizontal crash vector causes greater axial compression in the lumbar spine, followed by increasing flexion moment during torso pitch. To substantiate this theory, results from previous HBM studies have suggested that the lumbar spine experiences larger magnitudes of axial compression and flexion moment as recline angle increases [1-4]. However, compression-flexion lumbar spine loading and related injuries in frontal crashes have been reported for occupants seated in not only reclined postures [5-6], but also upright postures [7-11], as well as in field data where occupant position was not reported [12-19]. Thus, axial compression and flexion moment occur regardless of spinal recline posture and are suggested to be the primary loading mechanisms contributing to injury in frontal crashes. Further, the peak loads of interest have been shown to occur at different times during the crash [10,20]. Therefore, predicting human lumbar spine response to compression-flexion loading in HBMs is an important step towards being able to utilize the HBM lumbar spines with confidence and predict lumbar spine injury risk within the HBMs.

S. K. Tushak (skt5ay@virginia.edu) is a PhD student in Mechanical Engineering, B. D. Gepner is a Research Scientist, and J. R. Kerrigan is the Director and Associate Professor in Mechanical Engineering, all at the University of Virginia's Center for Applied Biomechanics, USA. B. Pipkorn is an Adjunct Professor at Chalmers University of Technology, Gothenburg, and Director of Simulation and Active Structures at Autoliv Research, Vårgårda, Sweden.

Likewise, not only should the HBM lumbar spine represent human behavior in injurious loading scenarios in which it is typically simulated in the injury biomechanics field, but it should also match the underlying characteristic responses to physiologic loading to capture the behavior when injury is not expected. Previously, HBM lumbar spines have been assessed relative to existing PMHS data to assess kinematic and kinetic responses [21,22]. However, these experimental data offer limited applicability due to complex boundary conditions, limited ranges of applied loads or displacements, or a lack of data needed to reproduce the experiments in HBMs. Thus, HBMs may be improved after assessments with new experimental data and loading that extends to higher magnitudes of compression and flexion that result in characteristic lumbar spine injuries observed in the field. In fact, recent component PMHS tests characterizing the lumbar spine in sub-injurious quasi-static loading in multiple directions [23] and injurious dynamic loading in compression-flexion [24] are now available, and HBMs have yet to be evaluated with this new data. This data is suitable for assessment of HBMs for mechanical characterization and future injury prediction. Therefore, the objective of this study was to evaluate the capability of the ligamentous GHBMC lumbar spine model to predict PMHS lumbar spine response for loading ranging from quasi-static to dynamic by implementing recent PMHS data.

II. METHODS

The GHBMC-O (v5.1.1) lumbar spine HBM with ligaments and intervertebral discs was selected for assessment. The v5.1.1 lumbar spine included updated tissue properties, enhanced intervertebral disc stability, and was the latest version available at the beginning of the study. A series of simulations were completed to compare model performance to the results from two different sets of post-mortem human subject (PMHS) lumbar spine component tests in different loading regimes. Accurately replicating the boundary conditions from the PMHS experiments was a goal of the study, so a description of the experimental boundary conditions, prescribed motion, and load/deformation measurements is included along with the implementation into the GHBMC simulations. All simulations were carried out in LS-DYNA (R12.0.0, mpp971, ANSYS).

Sub-Injurious: Quasi-Static Multi-Directional Characterization

Experiments

The GHBMC was first evaluated in sub-injurious loading regimes. The boundary conditions and loading curves from recent quasi-static tests characterizing PMHS ligamentous whole lumbar spine (T10-Sacrum) response in flexion/extension, lateral bending, torsion, anterior/posterior shear, and lateral shear with three levels of axial compression (0N, 900N, 1800N) [23] were implemented into LS-DYNA and are briefly described here. The T10-T12 and sacrum were secured in potting cups with wood screws and potting resin. Custom-made plastic collars reinforced with carbon fiber were rigidly affixed to the L1-L4 vertebrae and allowed for implementation of the follower load mechanism, which applied axial compression via two cables on lateral sides of the lumbar spine. The follower load allowed for anterior-posterior cable position to be adjusted separately at each vertebral level such that the vertebral center of rotation was approximated and axial compression was applied without off-axis loading and intra-vertebral rotations induced. Motion tracking markers were placed on each collar and on the L5 and were used for characterizing kinematics. A six-degree-of-freedom serial robot actuator arm supplied loads to the superior end about a pre-defined joint coordinate system (JCS) using a proprietary robotic control software, while the inferior end was fixed to the base (ground). The JCS was defined at the L4-L5 level and remained fixed in space for the duration of each test, and the spine moved with respect to the JCS during each test. Follower load application was achieved before initiating rotation/translation via two linear actuators on top of the robot that routed through the collars attached to the vertebrae, with load (0N, 900N, 1800N) distributed evenly between both. Parallel control schemes were used to move the robot arm in its primary loading axis in position control (i.e. prescribing translation or rotation), while utilizing force control (i.e. prescribing force/moment) in other axes to minimize force/moment in a desired axes to ensure pure bending or shear was applied to the spine. Further, the robot was instructed to find a path and position such that the force in the desired axes were zero. These desired axes had “released” boundary conditions and were unconstrained. For every direction, the robot applied follower load, moved the specimen in its test direction, held it in the final position for five seconds, and then returned the specimen to its neutral position. All kinetic data used for development of kinetic corridors (i.e. forces/moments via load cells and translations/rotations via motion tracking markers) were recorded in the JCS, but loads were transformed to the sacrum coordinate system (SCS) and position and deformations were recorded as superior

end translation/rotation with respect to the JCS. All kinematic data used for kinematic corridors (i.e. translations and rotations via motion tracking markers) were recorded as L1 and L5 deformations over the duration of the test with respect to their initial positions. Kinetic and kinematic corridors were created for each loading direction and axial compression level using arc-length parameterization for only the loading phase of each experimental test.

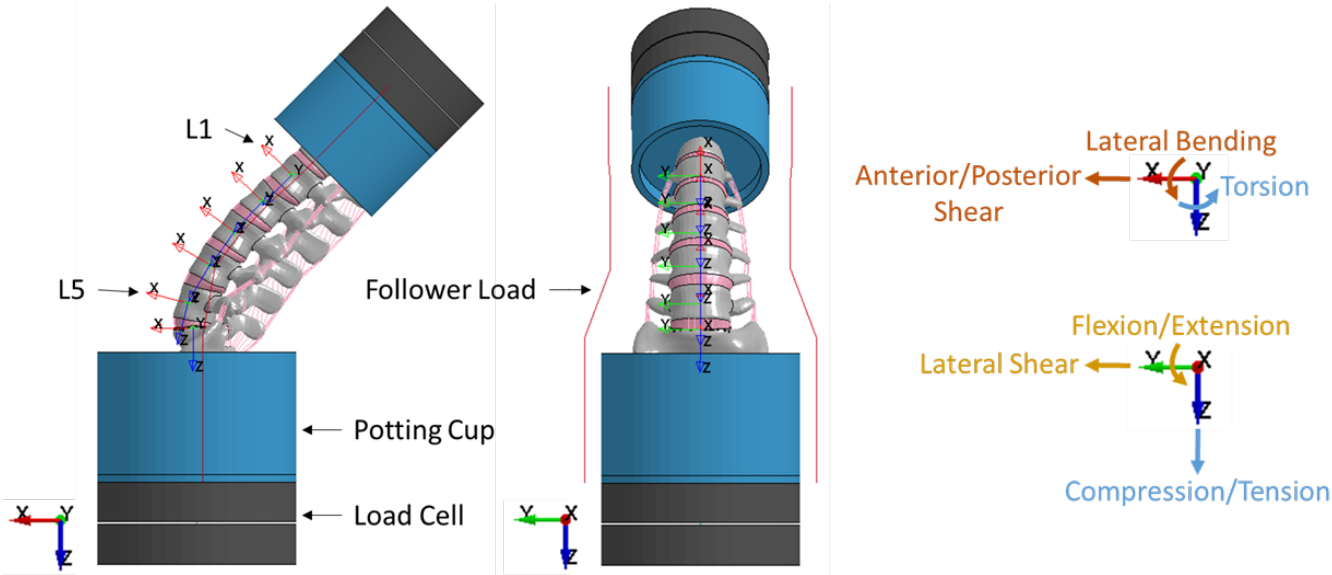

Fig. 1. Sub-injurious simulation setup with vertebral and global coordinate systems, in which the principal axes of the SCS were aligned with those of the global coordinate system. The description of axes related to primary loading directions is included on the right.

Simulations

To match previous PMHS experiments, a simplified setup of the experimental fixture was implemented, while maintaining the same boundary conditions (Figure 1). First, the GHBMC lumbar spine (T12-Sacrum) was rotated such that the SCS was aligned with the global xyz coordinate system. The SCS, each vertebral coordinate system (VCS), and the JCS were defined the same as in the PMHS experiments, by choosing three points on each endplate (anterior-most and right and left lateral-most points) and one point on each transverse process, and then calculating orthogonal axes via the ISB 2002 standard [25]. The VCSs were tied to and moved in conjunction with their respective vertebrae for the duration of each test, allowing for comparisons with the PMHS experiments. The SCS was fixed because the inferior potting cup and sacrum were fixed in place, similar to the experiments. The JCS was fixed in space since the JCS for robot system was defined once and remained stationary for each test. Then, the superior (T12) and inferior (L5) vertebrae were positioned in finite element models of the aluminum potting cups, concrete-like potting resin, and aluminum load cells used in the experiments. The sacrum superior endplate was parallel to the inferior potting cup, and the T12 inferior endplate was parallel to the superior potting cup, similar to the experiments. The superior and inferior cortical shell of the vertebrae was rigidly fixed to the deformable potting resin, and the potting resin was constrained to the rigid potting cups. Next, nodes were created on the right and left sides of each vertebral body to signify the location that the actuator cable routed through the vertebral collars, or the slipring location (positioned 74.9mm laterally from VCS origin). Each lateral node representing a slipring was tied (i.e. connected) to a set of four nodes on the lateral side of its corresponding vertebral body. Two 1D discrete beams were defined, one each on the left and right sides of the lumbar spine, connecting the slipring locations and representing the actuator cable which supplied the follower load. The cables extended length-wise to the potting cups and were tied to the potting cups with a similar definition as with the vertebrae.

Next, the superior potting cup was pre-flexed to 45 degrees with respect to the inferior potting cup to initially position the GHBMC, which was the average initial neutral lumbar curvature from the experiments (range: 35 to 60 deg). Initial stresses and strains were not incorporated since this posture was assumed to be the neutral position, similar to the experiments. Prescribed motion (rotation or displacement) was applied to the superior load cell, resulting in flexion/extension, lateral bending, torsion, anterior/posterior shear, and lateral shear, for the 0N follower load case first. Loading rate was equivalent to approximately 36deg or 40mm in 500ms. To mimic the robot's release of boundary conditions to minimize loads in the desired axes, the boundary conditions were

applied to the inferior and superior load cells via their material definition, and the appropriate degrees of freedom were defined (Table 1). Vertebral cross-sectional loads of 0N follower load simulations were checked to verify the boundary conditions matched those of the PMHS experiments (i.e. zero load in the "released" axes). The axial compression boundary condition was released for all load cases to allow for the application and preservation of the follower load via the cables. After 0N follower load simulations were complete, follower load was implemented to each cable with an initial force of either 0.45 or 0.90 kN (depending on the level of desired follower load), starting at time zero. Due to abrupt application of follower load in the simulations, the GHBMC experienced substantial vibrations. Damping was ramped up to a value of 0.1 and offset from the primary loading curve. Thus, the follower load was slowly applied over the first 100ms, before the prescribed motion began. Additionally, a global damping constant of 0.2 during the application of follower load and 0.01 for the remainder of the simulation was implemented. Just as with the experiments, the cable and slipring positions were adjusted in the anterior-posterior direction to minimize off-axis loads occurring from the application of follower load. Translating the nodes representing the sliprings 5mm posteriorly from the VCS origin in each local vertebral x-direction was the optimal cable position. Finally, the 900N and 1800N follower load cases were simulated with the same loading curves as with the 0N follower load cases. In this study, each of the HBMs was exercised in three different conditions representing various level of follower load axial force and eight loading directions utilized in the PMHS study. A full factorial design of experiments resulted in a total of 24 simulations (Table 1).

TABLE I
SIMULATION MATRIX FOR SUB-INJURIOUS TESTS

Primary Loading Direction	"Released" Axes	Follower Load Levels
Flexion	Compression, AP Shear	0N, 900N, 1800N
Extension	Compression, AP Shear	0N, 900N, 1800N
Lateral Bending	Compression, AP Shear, Lateral Shear	0N, 900N, 1800N
Torsion	Compression, AP Shear	0N, 900N, 1800N
Anterior Shear	Compression	0N, 900N, 1800N
Posterior Shear	Compression	0N, 900N, 1800N
Lateral Shear	Compression, AP Shear	0N, 900N, 1800N

GHBMC responses were compared to PMHS kinetic and kinematic corridors. Kinetic corridors described the load-deformation responses, while kinematic corridors described relative motions of vertebrae. Only kinematic and kinetic measurements in each test direction's primary loading direction was considered. In the case of tests with follower loads, the response was plotted after the follower load was applied, starting at the initiation of prescribed motion. For comparison with kinetic corridors, loads were measured in 1D discrete beam elements located at the representative sensing plane of the experimental load cells (approximately half the height of the load cell). Loads were transformed from the 1D beam elements to the SCS so that responses could be directly compared to those from the PMHS experiments. Since the xyz axes of these coordinate systems were aligned, only a static translation transformation was necessary to translate the loads by [2.9, 0, -162.5]mm. Translation or rotation was measured as the center of the outside face of superior potting cup relative to the JCS origin, similar to the end effector relative to the JCS in the experiments. For equivalent comparisons with kinematic corridors, relative translation/rotation of the L1 and L5 vertebrae were calculated for all simulations (i.e. L1 motion relative to its initial position).

Injurious: Dynamic Compression-Flexion Characterization

Experiments

The GHBMC was secondly evaluated in injurious loading related to MVCs. A previous PMHS study assessed lumbar spine injuries in combined compression and flexion loading by first quasi-statically applying one of three pre-determined levels of axial compression to three-vertebrae segments (T12-L2; L3-L5), and then flexing the segments at a high-rate to failure [24]. The test series utilized a test fixture that applied controlled rotation to the superior end of the segment, while releasing the anterior-posterior constraint via a linear rail that allowed for anterior-posterior translation. The result was pure moment throughout the spine in which the magnitude of flexion moment along the length of the segment was altered by the axial compression. The distal halves of the superior and inferior vertebrae were secured to the potting cup via a rigid pedestal, wood screws, and concrete-

like potting resin to keep the posterior elements intact, to allow for precise positioning on the test fixture, and to maintain hold during high-rate flexion. The specimens were positioned in the test fixture such that the superimposed axial compression force was applied perpendicular to the mid-plane of the middle vertebrae via a spring-honeycomb system, where compressing the spring translated to force against the honeycomb and axial compression was placed on the spine. The system was used to maintain approximately a constant force of one of three levels (2200 N, 3300 N, 4500 N) throughout dynamic flexion. The center of rotation was chosen as the inferior-most endplate of the segment to minimize motion on the linear rail and reduce the effect of inertial constraints. Further, translation along the linear rail and translation associated with the honeycomb crushing to maintain constant axial force allowed for the instantaneous adjustment of the center of rotation about the segment, even though the laboratory-defined center of rotation about the test fixture remained fixed. Loads were transformed from the load cell coordinate system and position to the middle vertebrae coordinate system and position, taking into account the bending moment induced by the axial compression and inertial compensation. Gross angle of the segments was quantified as the superior end rotation with respect to its initial position (i.e. flexion angle). Only moment-angle response was considered until the first reported injury occurred, as response after injury would be influenced by the loads transmitted through an unstable structure.

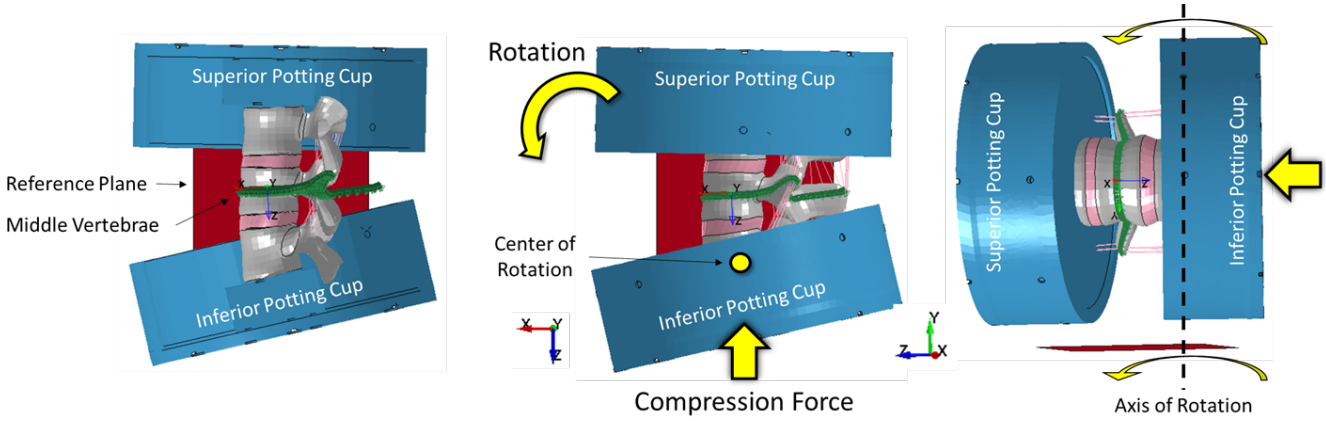

Fig. 2. Injurious simulation setup with the middle vertebrae and global coordinate systems, in which the principal axes were aligned, and with the cross-section in which loads were measured.

Simulations

To match previous PMHS experiments, the GHBMC was split into three-vertebrae segments (T12-L2; L3-L5). A simplified setup of the experimental fixture was implemented, while maintaining the same boundary conditions (Figure 2). Two initial positions were considered for each T12-L2 and L3-L5 segment since segment curvature varied among the PMHS (T12-L2 average: 3 deg, range: -9 to 14 deg; L3-L5 average: 25 deg, range: 17 to 34 deg where positive curvature is spinal lordosis and negative curvature is spinal kyphosis), yielding four HBMs for simulation (Figure 3). The “occupant” representative positions were the baseline positions for the GHBMC segments. The “pedestrian” representative positions were approximated from the spinal alignment of a pedestrian HBM (THUMS v.4.01.). The occupant position was positioned to the target pedestrian positions via FE simulation. All simulations began without pre-stress/strain.

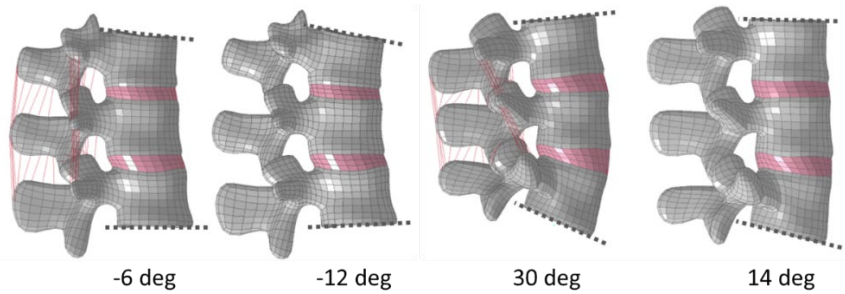

Fig. 3. Pedestrian (first and third) and occupant (second and fourth) postures for T12-L2 (left) and L3-L5 (right) lumbar spine segments.

The lumbar segments were rotated such that the mid-plane of the middle vertebrae, defined as the mid-plane

between the superior and inferior endplate, was aligned with the global xyz coordinate system. Then, the superior (T12; L3) and inferior (L2; L5) vertebrae were positioned in finite element models of the aluminum potting cups and pedestal blocks, concrete-like potting resin, and aluminum load cells used in the experiments. The potting definitions and constraints were modelled the same as for the sub-injurious simulation setup. Next, a reference rigid body was created and constrained in all degrees of freedom to represent the PMHS test fixture attachment reference. The rotating superior end was constrained with the reference rigid body utilizing a cylindrical joint definition, thus replicating the laboratory-fixed center of rotation. Similar to the experimental setup, the global axis of rotation location was chosen at the inferior-most endplate of the segment to minimize the inferior potting cup motion and to reduce the influence of the inertial boundary forces. The inferior potting cup was constrained in all rotations, and its translational motion was released in anterior-posterior and superior-inferior directions to replicate the linear rail and axial preload/crushing mechanisms, respectively. Finally, the axial compression force was applied at the beginning of the simulation and maintained throughout the simulation. The axial compression was applied in the global z-direction, which was aligned with the mid-plane of the middle vertebrae. A global damping constant of 0.2 was implemented during the application of axial compression and then removed for the remainder of the simulation. The superior potting cup was driven using a representative experimental input pulse of the superior potting cup angular velocity. In this study, each of the proposed HBMs was exercised in three different conditions representing various level of superimposed axial compression force utilized in the PMHS study (2200N, 3300N, and 4500N). A full factorial design of experiments resulted in a total of 12 simulations including various levels of axial compression, lumbar anthropometry, and initial position (Table 2). Each of the 12 models exercised in this study was evaluated with respect to individual moment-angle responses from the experiments. Loads were measured in the middle vertebrae cross-section representing the mid-plane. Loads were reported with respect to the vertebrae coordinate system (middle of the vertebral body) so they could be directly compared to those from the PMHS experiments. When doing this, the flexion moment was adjusted for the measured axial force multiplied by its moment arm between the centroid of the vertebral cross-section and the origin of the vertebral coordinate system. Angle of the superior potting cup relative to its initial position was extracted over the duration of the simulations. The HBMs were compared to their appropriate experimental data counterpart: T12-L2 and L3-L5 separated by compression level (2200N, 3300N, 4500N) for a total of six comparisons. The six experimental tests in which the segment failed during the application of compression did not have response curves and were therefore not considered for evaluation and comparison.

TABLE 2
SIMULATION MATRIX FOR INJURY TESTS

Lumbar Section	Initial Position	Axial Compression Force
T12-L2	Occupant	2200N, 3300N, 4500N
L3-L5	Pedestrian	

Model Evaluation

The GHBMC was evaluated relative to the PMHS data by comparing the stiffness coefficients and the linearity constant. In both sets of PMHS data, the majority of kinetic responses displayed a bilinear behavior, in which there were two distinct regions (toe region of lower stiffness followed by a loading region of higher stiffness with engagement of the structures). This bilinear behavior was characterized by splitting the two regions with straight lines whose slopes represent stiffness coefficients. The ratio of the two stiffness coefficients represented the linearity constant of the response, quantifying how linear or non-linear the entire response is over the range of rotation or displacement. The stiffness coefficients for the sub-injury PMHS data had been previously reported and compared among follower load levels and loading directions [23] using a method proposed by [26]. The average stiffness values from the PMHS tests were digitized from [23]. To compare how GHBMC stiffness values changed with the addition of axial compression, two linear regressions were performed with pre-defined ranges of data (Table C1), similar to the statistical method in the sub-injury experiments. Then, the linearity constants were calculated from the stiffness coefficients, which was the ratio of the stiffness of the first region to the stiffness of the second region.

A similar approach to quantify stiffness coefficients and linearity constants was performed in this study on the PMHS injury data. Two linear regressions (i.e. piecewise linear regression) were utilized to approximate the slopes of both regions, in which each injury response curve until the point of first fracture was split into two regions and

simultaneously fit across all values of rotation or displacement. The inflection point, or the point in which the higher-stiffness region began, was determined as the rotation or displacement in which the least squares of both regressions were minimized. The regression treated the response curve as continuous, so both lines resulting from the linear regression were connected at the inflection point. The linearity constants were calculated from the stiffness coefficients. Similarly, stiffness coefficients and linearity constants were calculated for all HBM responses, most of which exhibited linear behavior.

Few sub-injury PMHS mean responses and injury PMHS tests exhibited one stiffness region. In which case, only one regression was performed, resulting in one stiffness coefficient and a linearity constant of 1 (i.e. perfectly linear). Again, these were previously reported for sub-injury data, but were determined for injury data and all GHBMC simulations in this study. For PMHS and GHBMC response curves, a bilinear regression was performed first. If the inflection point was at the beginning or end of the response curve and the response curve did not display two distinct regions, then a linear regression was performed and used thereafter for comparisons between PMHS and HBMs. Student's paired t-tests were performed to determine significant differences in stiffness values, linearity constants, and points of inflection between both regions of the bilinear response curves and between levels of axial compression of the PMHS injury data. GHBMC stiffness values were compared to their PMHS counterparts.

III. RESULTS

Sub-Injurious: Quasi-Static Multi-Directional Characterization

For sub-injurious cases with no axial compression, the GHBMC responses were within the bounds of the kinetic PMHS corridors in flexion, lateral bending, torsion, and posterior shear and exhibited a similar behavior (Figures 4, A1). However, the GHBMC was stiffer in lateral shear (GHBMC = 505 N; PMHS = 186 N at 40 mm displacement) and anterior shear (GHBMC = 380 N; PMHS = 134 N at 40 mm displacement) and was more compliant in extension (GHBMC = 3 Nm; PMHS = 19 Nm at 15 deg rotation) (Figure A1). The GHBMC was within the bounds of all PMHS kinematic corridors except for flexion, where it exhibited half the L5 rotation for a given L1 rotation (GHBMC = 5 deg; PMHS = 10 deg at 20 deg L1 rotation) (Figure A1). In most cases, increasing axial compression minimally affected model response, stiffness, and linearity constant, unlike most PMHS cases (Figures 4, A1; Tables C2, C3).

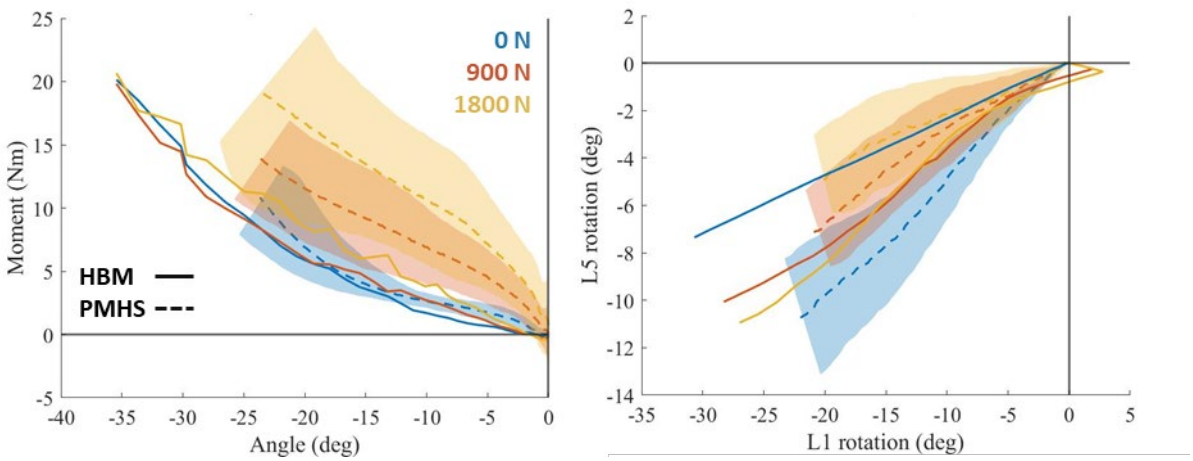

Fig. 4. Flexion GHBMC simulation (solid lines) kinetic (left) and kinematic (right) responses compared to PMHS mean (dashed lines) and corridors (shaded regions) for three levels of follower load—0 N (blue), 900 N (orange), and 1800 N (gold) [21]. GHBMC curves are plotted for the duration of the simulation. Plots of other loading directions can be found in the Appendix.

Overall, the GHBMC responses were the most nonlinear at lower levels of follower load, with increased linearity at 1800 N of follower load. This trend matched that of the PMHS, although the majority of linearity constants themselves were not similar to those of the PMHS for each loading direction and level of follower load.

Injurious: Dynamic Compression-Flexion Characterization

The GHBMC and PMHS responses were within the same range (0 to 40 deg of rotation, -5 to 181 Nm of flexion) for each combination of segment and axial compression (Figure 5). The GHBMC responses were linear (average

stiffness = 2.63 Nm/deg) (Table C5). All but three PMHS responses displayed bilinear behavior with a flatter region (average slope = 0.89 Nm/deg) followed by a stiffer region (average slope = 8.46 Nm/deg), with an average point of inflection of 14 degrees (Table B4). The average stiffness of these two regions were significantly different from one another ($p << 0.001$), as well as significantly different from the GHBMC average stiffness ($p << 0.001$). The average stiffness in both bilinear regions did not significantly vary by segment or compression level ($p > 0.18$ for all). The linearity constants calculated from the PMHS stiffness values corroborated nonlinear response behavior (average ratio = 0.11). The stiffness of the three linear PMHS responses (average stiffness = 1.84 Nm/deg) were not significantly different from the average stiffness of the GHBMC responses ($p = 0.21$).

The occupant and pedestrian responses were similar for the T12-L2 segment, but the responses of the two HBMs deviated for the L3-L5 segment (Figure 5). However, the responses of both HBMs do not substantially change with increases in axial loads of 2200 to 4500 N, except for different initial moment values among the three levels of axial compression (Figure B1). Yet, average GHBMC stiffness did not significantly vary by segment, position, or compression level ($p > 0.11$ for all).

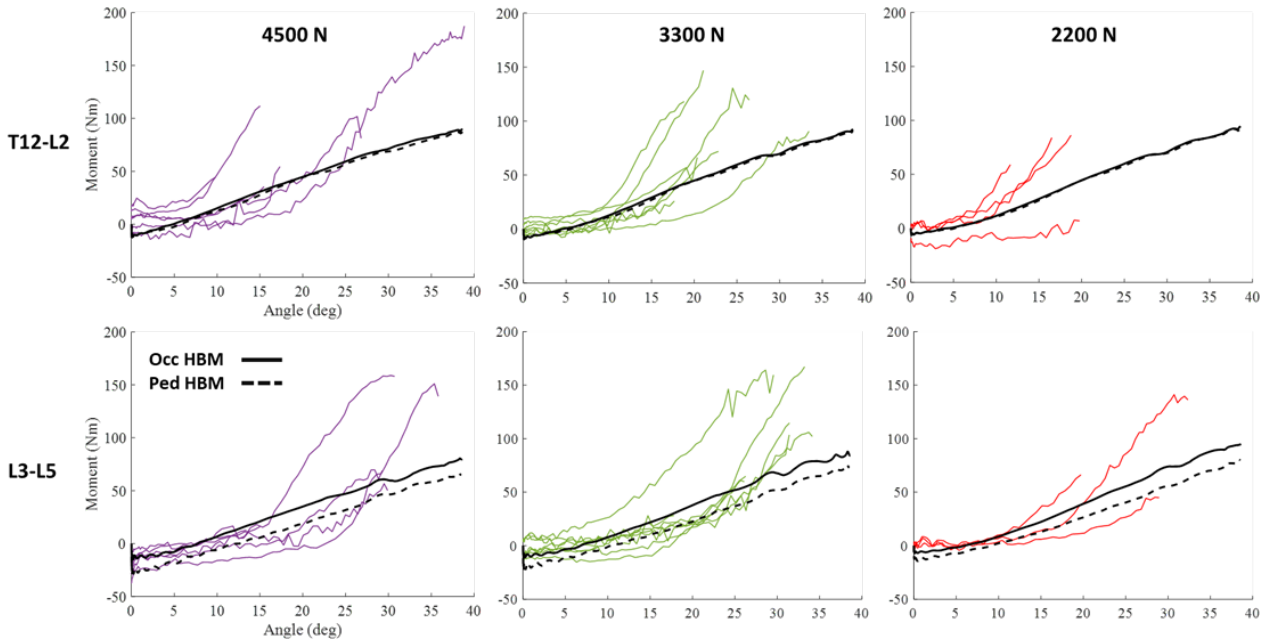

Fig. 5. Occupant (solid black lines) and pedestrian (dashed black lines) GHBMC simulation moment-angle stiffness responses compared to individual PMHS response curves, separated by T12-L2 (top) and L3-L5 (bottom) segments and by compression level—4500 N (left, purple), 3300 N (middle, green), and 2200 N (right, red). PMHS curves are plotted up until the point of first fracture. GHBMC curves are plotted for the duration of the simulation.

IV. Discussion

The objective of this study was to evaluate the GHBMC lumbar spine performance compared to the recent PMHS data to understand current GHBMC loading and kinematic behavior relative to the experiments. Responses varied among both experimental datasets and by loading directions and/or compression load levels. Fundamentally, the lumbar spine's structural mechanical response to sub-injurious loading is at least partially dictated by the soft tissues surrounding the vertebrae (i.e. the ligaments and the intervertebral discs). For instance, in flexion, the posterior ligaments are loaded in tension and the disc, particularly the anterior portion of the disc, is loaded in compression. Since the ligaments and discs have substantially lower stiffness than the vertebrae, at least a portion of the moment-angle response is determined by the material response of these soft tissues. The posterior ligaments (posterior longitudinal ligament, ligamentum flavum, interspinous ligament, supraspinous ligament), in particular, have relatively large moment arms due to their positions relative to the spine's neutral axis in flexion. However, when axial compression of the spine is superimposed during flexion, or when the spine is subjected to extension, lateral shear or anterior shear, the facet joints are compressed and engaged, which may introduce a secondary load path that could offset or mitigate ligament loading and stiffen the load-deformation response. This behavior was displayed primarily in the sub-injury experimental tests, in

which the addition of axial compression caused increased stiffness. However, this behavior was not observed in the GHBMC in the majority of load cases.

Since the location of the ligaments relative to the neutral axis affects response, the stiffness, or material properties, of the ligaments also plays a role in overall response. The ligament curves in the model were defined with three regions: lower stiffness, higher stiffness, lower stiffness (Figure D1). The first two regions likely represent the toe-region, and then a stiffening response of the structures (which is commonly seen in soft biological tissues). The third region, which exhibits strain-softening, appears to be pre-failure damage, as observed individual ligament tensional tests [27]. The GHBMC ligaments consist of multiple fiber bundles (i.e. multiple 1D beam elements) per ligament, and the same material definition is defined for all fiber bundles of the same ligament. Thus, the stiffness of the fiber bundles is governed by the area of the fiber bundle (i.e. number of 1D beam elements). The lumbar spine model was validated against several functional spinal unit and whole lumbar spine PMHS tests [21], but the specifics on the ligament material formulation and implementation was not clear. Previous studies that have implemented several ligament material datasets into a single lumbar spine model have displayed that large variations in ligament-strain relationships between datasets causing varied responses of the model [28, 29]. Therefore, the ligament data chosen to be implemented in the GHBMC lumbar spine would have a large influence on the resulting load-deformation responses, and those responses may be different if another set of ligament data was used instead. Further analysis as to the sensitivity of different ligament datasets on the GHBMC responses relative to the experimental validation suite can be performed.

In the simulations of the injurious tests, the ligaments surpassed the elongation limits defined in the ligament response curves (Figure D1), and the ligament responses of the GHBMC were linearly interpolated after curve definition ended, with the same stiffness slope as the third region. Thus, the ligament responses, particularly in the injurious tests in which lumbar segments are flexed to large angles at high rates, may not accurately represent ligament behavior in the spinal unit due to being too compliant at larger flexion angles. Further, ligaments are suggested to play an important role in resisting larger moments, so their accurate representation can improve validity of the model [29]. Similarly, the intervertebral discs play a role in resisting loads applied to the lumbar spine, so the material properties in the GHBMC can largely affect the resulting moment response. The current definition of the annulus fibrosis and nucleus are hill foam, elastic fluid, and fabric with the moduli definitions dictating the material stiffness. The differences between the PMHS and GHBMC responses could be due in part to both the ligaments and the intervertebral discs. To the authors' knowledge, previous experimental studies describing compression-flexion of the spine to large angles at high rates have not been available, so the GHBMC may not have been exercised in similar conditions to discover the challenges with the ligaments and discs related to large rotation angles in multi-segment lumbar spine units.

Along with ligament and intervertebral disc definitions affecting the mechanical response of the GHBMC, the geometry of the GHBMC can also affect the loads placed on the vertebrae. The cross-sectional area (CSA) of the middle vertebrae superior endplates of the GHBMC segments were calculated following the method used in the PMHS injury study and were compared to a distribution of PMHS CSAs measured from CT scans. In all cases, the GHBMC CSA was larger than the mean of the distribution from each comparison group (Figure D2). The difference in CSA could be partially explained by the fact that the GHBMC anthropometry is that representing a 50th percentile male, and that the PMHS study included several smaller female specimens. However, controlling for female specimens also shows that the GHBMC lumbar model was larger than an average male specimen used in this study. A larger CSA likely corresponds to smaller stresses measured within the vertebral body for a given axial compression force and flexion moment. Among other geometrical measures of interest could be vertebrae anterior-posterior length, which influences ligament moment arm, as well as ligament initial length. Lastly, the initial position (i.e. spinal curvature, lordosis/kyphosis angle) could dictate loading within the vertebrae and the resulting stiffness response. In this study, the GHBMC occupant and pedestrian HBMs did not show substantially different stiffness and response when varying the initial position. The occupant postures generally represented spinal segments with larger kyphosis (T12-L2) and smaller lordosis (L3-L5), while the pedestrian postures generally represented spinal segments with smaller kyphosis (T12-L2) and larger lordosis (L3-L5), measured as the sagittal angle between the superior-most endplate and the inferior-most endplate. Negative moments were observed in both the experiments and simulations when the preload was applied and indicated extension in the spinal segments. In the simulations, the magnitude of extension for the four HBM postures varied and is likely due to how the curvature of the spinal segments were aligned. However, the PMHS sensitivity to initial position needs

to be investigated before commenting on the biofidelity of the GHBMC in this specific aspect. Overall, a deeper analysis is required to understand how ligament and intervertebral disc properties, geometry, and initial position affect the resulting responses and loads measured in the lumbar spine.

Exercising a HBM in numerous loading conditions at once can lead to poor performance in one or more of these scenarios. The expectation that the HBM will match PMHS response in all of these loading conditions might be unrealistic. Thus, incorporating PMHS data for loading scenarios that are most relevant to the field into the existing validation suite may be beneficial for improving the GHBMC lumbar spine component biofidelity. The authors are not suggesting that a HBM cannot be biofidelic in all the considered loading conditions, no matter how numerous they are. However, a first step in improving the utility of the HBM could be to optimize a few relevant loading scenarios first. In the case of the GHBMC, the ligament and intervertebral disc properties may pose as primary contributors as to why the GHBMC behavior and stiffness may not adequately match the PMHS in some loading conditions. Thus, after further investigation, ligament or intervertebral disc properties may need to be altered to improve the model. A first step could be to optimize them such that the compression-flexion responses and behavior in sub-injurious and injurious loading better match those of the PMHS data used in this study, and potentially other previously published PMHS data. Additionally, although some of the GHBMC kinematic responses matched those of the PMHS well (i.e. were within the PMHS corridors), the kinetic responses for the same loading directions did not necessarily perform similarly as well based on the calculated stiffness coefficients and corridors. For example, the GHBMC kinematic response in extension is close to the PMHS mean for all three levels of axial compression, but the kinetic response is more compliant and does not change with the addition of axial compression. This shows that kinematic or kinetic response alone cannot be used to accurately evaluate and validate a HBM, at least in the loading conditions included in this study; they must both be considered. Further, even if the kinematics are correct, the loading within the cross-section may be incorrect and therefore affect the resulting injury risk prediction by over- or under-estimating injury risk if the loads are too high or too low compared to PMHS data. Similarly, even if the loads measured in the cross-section are representative of humans, the motion of the vertebrae relative to each other must be realistic for the given measured loads.

It should be noted that only one baseline HBM was selected (GHBMC), and comments of how other HBMs (e.g. THUMS or SAFER) and anthropometries (i.e. scaling) compare to the PMHS data cannot be included without their own similar investigations; the difference in results among HBMs may be due to differences in HBM-specific biofidelity or geometry. Similarly, this study evaluated a component lumbar spine in specific loading conditions and cannot be extrapolated to the whole-body response and other loading scenarios without further investigations. Lastly, since the completion of the study the v6.0.0 model has been released and includes minimal changes to the lumbar spine, namely alterations in cortical thickness and material card, additional and updated parameters, and removal of erosion in the nucleus.

V. CONCLUSIONS

Recently published PMHS lumbar spine data was utilized to evaluate the response of the GHBMC lumbar spine. The evaluation shed light on the performance of the GHBMC when exercised in multiple sub-injurious, quasi-static loading directions with three levels of axial compression and injurious compression-flexion loading at high rates. The outcomes from this study can contribute to describing the utility of the existing GHBMC lumbar spine. Generally, the GHBMC and PMHS did not respond similarly when increased levels of axial compression were applied in both sub-injurious and injurious loading cases. Additionally, the GHBMC did not display the same bilinear response that most PMHS displayed. Further investigation is necessary to divulge what is causing the discrepancy between the GHBMC and PMHS behavior and stiffness (e.g. ligament properties, geometry, spinal curvature).

VI. ACKNOWLEDGEMENT

Funding for this research was provided by Autoliv. It should be noted that the views or opinions expressed here are those of the authors and not necessarily aligned with the views and opinions of the sponsoring organization.

VII. References

[1] Boyle KJ, Reed MP, Zaseck LW, Hu J. A Human Modelling Study on Occupant Kinematics in Highly Reclined Seats during Frontal Crashes. *Proceedings of the IRCOBI Conference*, 2019, Florence, Italy

[2] Rawska K, Gepner BD, et al. Submarining sensitivity across varied anthropometry in an autonomous driving system environment. *Traffic Injury Prevention*, 2019, 20(sup2):S123-S127.

[3] Tang L, Zheng J, Hu J. A numerical investigation of factors affecting lumbar spine injuries in frontal crashes. *Accidental Analysis and Prevention*, 2020, 136(105400).

[4] Katsuhara T, Takahira Y, Hayashi S, Kitagawa Y, Yasuki T. Analysis of Driver Kinematics and Lower Thoracic Spine Injury in World Endurance Championship Race Cars during Frontal Impacts. *SAE International Journal of Transportation Safety*, 2017, 5(1):120-132.

[5] Richardson R, Donlon JP, et al. Kinematic and Injury Response of Reclined PMHS in Frontal Impacts. *Stapp Car Crash Journal*, 2020a, 64:83-153.

[6] Richardson R, Jayathirtha M, et al. Thoracolumbar Spine Kinematics and Injuries in Frontal Impacts with Reclined Occupants. *Traffic Injury Prevention*, 2020b, 21(sup):S66-S71.

[7] Begeman PC, King AI, Prasad P. Spinal Loads Resulting from -Gx Acceleration. *Proceedings of Stapp Car Crash Conference*, 1973, Coronado, CA.

[8] Patrick LM, Levine RS. Injury to Unembalmed Belted Cadavers in Simulated Collisions. *Proceedings of Stapp Car Crash Conference*, 1975, San Diego, CA.

[9] Rouhana SW, Bedewi PG, et al. Biomechanics of 4-Point Seat Belt Systems in Frontal Impacts. *Stapp Car Crash Journal*, 2003, 47(2003-22-0017):367-399.

[10] Uriot J, Potier P, Baudrit P, Trosseille X, Richard O, Douard R. Comparison of HII, HIII and THOR dummy responses with respect to PMHS sled tests. *Proceedings of the IROCBI Conference*, 2015, Lyon, France.

[11] Kallieris D, Mattern R, Schmidt G, Warth D. Kinematic and Spinal Column Injuries in Active and Passive Passenger Protection Results of Simulated Frontal Collisions. Proceedings of the IRCOBI Conference, 1984, Delft, The Netherlands.

[12] Doud AN, Weaver AA, et al. Has the incidence of thoracolumbar spine injuries increased in the United States from 1998 to 2011? *Clinical Orthopaedics and Related Research*, 2015, 473(1):297-304.

[13] Kaufman RP, Ching RP, Willis MM, Mack CD, Gross JA, Bulger EM. Burst fractures of the lumbar spine in frontal crashes. *Accident Analysis and Prevention*, 2013, 59:153-163.

[14] Pintar FA, Yoganandan N, Maiman DJ, Scarboro M, Rudd RW. Thoracolumbar spine fractures in frontal impact crashes. Annals of advances in automotive medicine. *Proceedings of the AAAM Conference*, 2012, 56:277-283.

[15] Wang MC, Pintar FA, Yoganandan N, Maiman DJ. The continued burden of spine fractures after motor vehicle crashes. *Journal of Neurosurgery: Spine*, 2009, 10:86-92.

[16] Adolph T, Wisch M, et al. Analyses of Thoracic and Lumbar Spine Injuries in Frontal Impacts. *Proceedings of the IRCOBI Conference*, 2013 Goteborg, Sweden.

[17] Huelke DF, Mackay GM, Morris A. Vertebral Column Injuries and Lap-Shoulder Belts. *Journal of Trauma*, 1995, 38(4):547-556.

[18] Jakobsson L, Bjorklund M, Westerlund A. Thoracolumbar Spine Injuries in Car Crashes. *Proceedings of the IRCOBI Conference*, 2016, Malaga, Spain.

[19] Shaikh J, Thathia H, Lubbe N. Lumbar Spine Injuries in Motor Vehicle Crashes. *Proceedings of the IRCOBI Asia Conference*, 2020, Beijing, China.

[20] Gepner BD, Draper D, et al. Comparison of Human Body Models in Frontal Crashes with Reclined Seatback. *Proceedings of the IRCOBI Conference*, 2019, Florence, Italy.

[21]GHBMC M50-O Documentation Users' Manual, released with each version of the model. Global Human Body Models Consortium, LLC.

[22] THUMS Documentation Users' Manual, released with each version of the model. Toyota Motor Company.

[23]Chastain KL. Characterization of the Mechanical Response of the Lumbar Spine: The Effect of a Compressive Axial Load. *Master's Thesis for the University of Virginia*, 2021. https://libraetd.lib.virginia.edu/public_view/m613mz49w

[24]Tushak SK, Donlon JP, et al. Failure Tolerance of the Human Lumbar Spine in Dynamic Combined Compression and Flexion Loading. *Journal of Biomechanics*, 2022, 135:111051.

[25]Wu G, Siegler S, et al. ISB recommendation on definitions of joint coordinate system of various joints for the reporting of human joint motion—part I: ankle, hip, and spine. *Journal of Biomechanics,* 2002, 35: 543-548.

[26]Patwardhan AG, Havey RM, et al. Effect of compressive follower preload on the flexion–extension response of the human lumbar spine. *Journal of Orthopaedic Research*, 2003, 21(3):540-546.

[27]Chazal, 1985

[28]Damm N, Rockenfeller R, Gruber K. Lumbar spinal ligament characteristics extracted from stepwise reduction experiments allow for preciser modeling than literature data. *Biomechanics and Modeling in Mechanobiology*, 2020, 19:893-910.

[29]Naserkhaki S, Arjmand N, Shirazi-Adl A, Farahmand F, El-Rich M. Effects of eight different ligament property datasets on biomechanics of a lumbar L4-L5 finite element model. *Journal of Biomechanics*, 2018, 70:33-42.

VIII. APPENDIX

Appendix A: Comparison of the GHBMC response to PMHS sub-injury kinetic and kinematic corridors

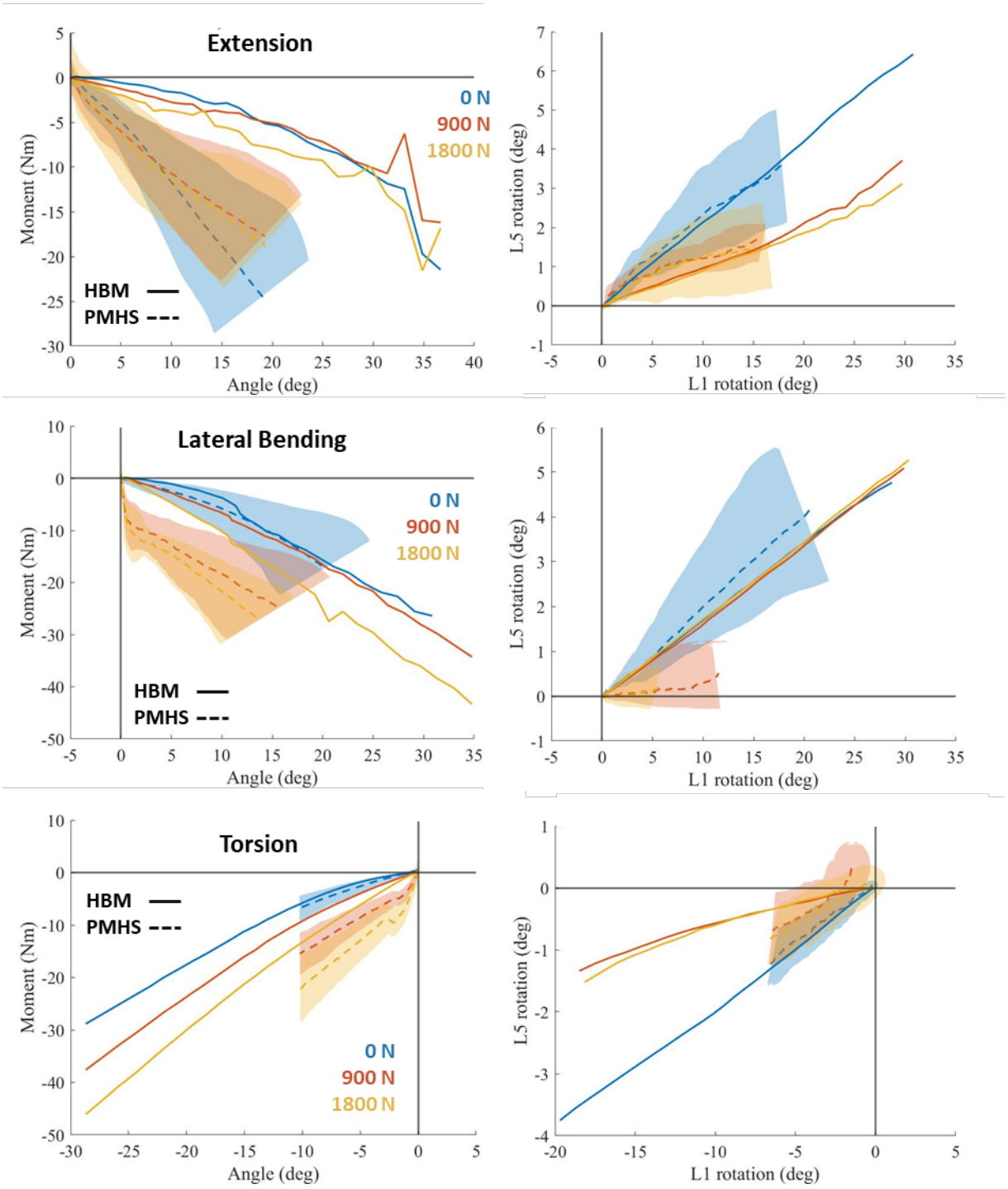

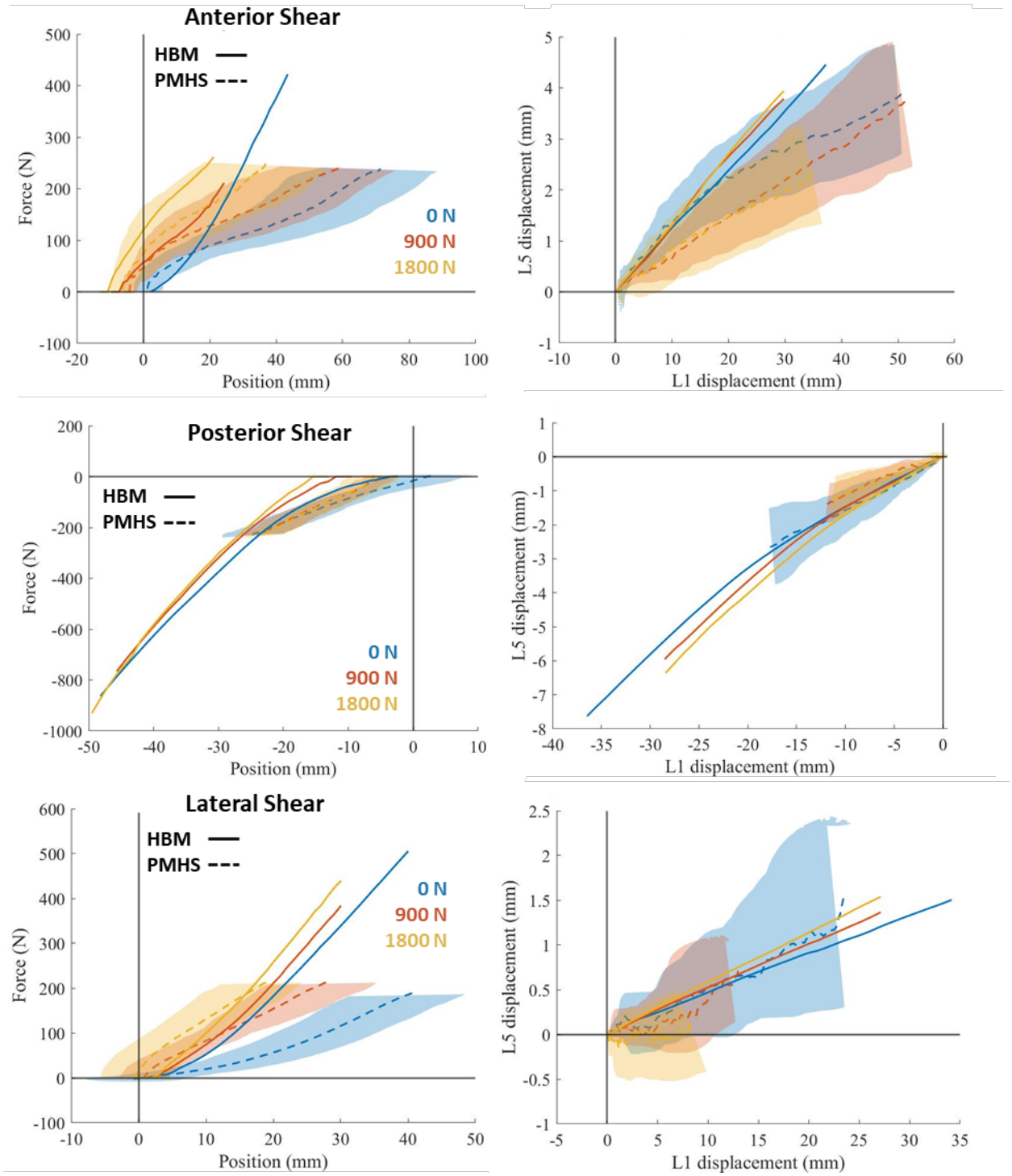

Fig. A1. HBM simulation (solid lines) kinetic (left) and kinematic (right) responses compared to PMHS mean (dashed lines) and corridors (shaded regions) for three levels of follower load—0 N (blue), 900 N (orange), and 1800 N (gold) [23]. HBM curves are plotted for the duration of the simulation.

Appendix B: Comparison of the GHBMC responses from injurious loading simulations

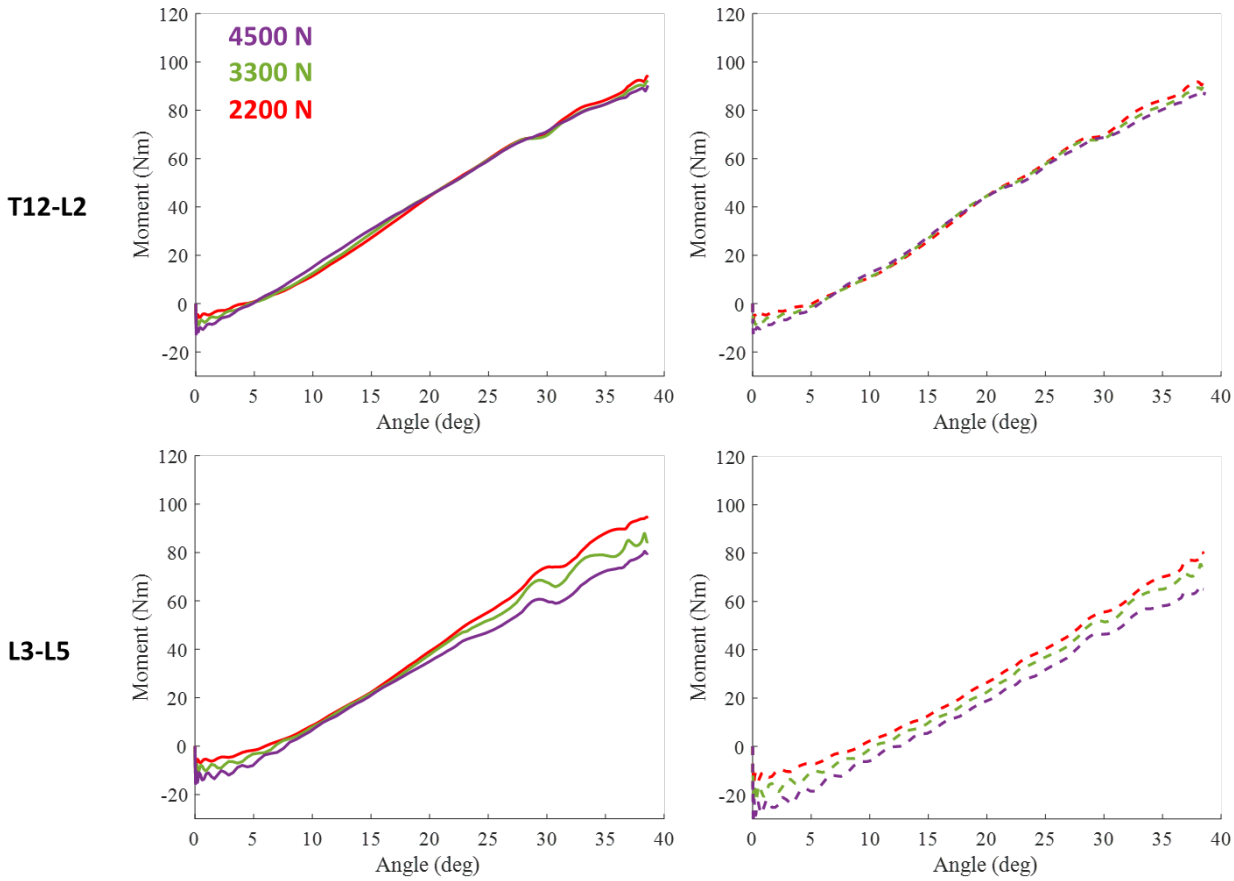

Fig. B1. Occupant (left) and pedestrian (right) HBM simulation moment-angle responses at three levels of axial compression.

Appendix C: Stiffness coefficients and linearity constants

TABLE C1
LIMITS OF RANGES USED FOR SUB-INJURIOUS LINEAR REGRESSIONS TO DETERMINE STIFFNESS COEFFICIENTS

	Flexion (deg)	**Extension** (deg)	**Lateral Bending** (deg)	**Torsion** (deg)	**Anterior Shear** (N)	**Posterior Shear** (N)	**Lateral Shear** (N)
S1	5-10	2-5	4-7	3-6	0-120	0-75	0-75
S2	15-end	7-end	8-end	7-end	150-end	150-end	150-end

TABLE C2
CALCULATED STIFFNESS VALUES FOR THE PMHS SUB-INJURY TESTS

		Flexion	**Extension**	**Lateral Bending**	**Torsion**	**Anterior Shear**	**Posterior Shear**	**Lateral Shear**
S1	**0 N**	0.18	1.02	0.52	0.73	3.31	9.00	3.10
(N/mm;	**900 N**	0.54	1.04	1.23	1.34	6.35	13.06	9.20
Nm/deg)	**1800 N**	0.71	1.15	1.41	2.00	11.81	16.98	15.57
S2	**0 N**	0.86	1.44	1.06	0.93	4.96	10.29	5.73
(N/mm;	**900 N**	0.59	0.77	1.1	1.42	4.27	13.98	7.06
Nm/deg)	**1800 N**	0.78	0.71	1.61	1.83	5.38	13.85	8.46
Linearity	**0 N**	0.21	0.71	0.49	0.78	0.67	0.87	0.54
Constant	**900 N**	0.92	1.35	1.12	0.94	1.49	0.93	1.30
(-)	**1800 N**	0.91	1.62	0.88	1.09	2.20	1.23	1.84

TABLE C3
CALCULATED STIFFNESS VALUES FOR THE SIMULATION SUB-INJURY TESTS

		Flexion	**Extension**	**Lateral Bending**	**Torsion**	**Anterior Shear**	**Posterior Shear**	**Lateral Shear**
S1	**0 N**	0.22	0.18	0.43	0.56	7.03	7.37	8.39
(N/mm;	**900 N**	0.34	0.24	0.75	0.94	5.49	13.04	9.82
Nm/deg)	**1800 N**	0.43	0.34	1.11	1.36	9.58	16.88	12.69
S2	**0 N**	0.83	0.45	1.09	1.21	13.02	25.11	16.08
(N/mm;	**900 N**	0.73	0.35	1.08	1.49	8.92	26.60	17.05
Nm/deg)	**1800 N**	0.67	0.45	1.31	1.72	5.98	29.48	17.99
Linearity	**0 N**	0.27	0.40	0.40	0.46	0.54	0.29	0.52
Constant	**900 N**	0.46	0.70	0.70	0.63	0.62	0.49	0.58
(-)	**1800 N**	0.63	0.75	0.85	0.79	1.60	0.57	0.71

TABLE C4
CALCULATED STIFFNESS VALUES FOR THE PMHS INJURY TESTS

ID	**Segment**	**Compression Level** (N)	**Slope 1** (Nm/deg)	**Slope 2** (Nm/deg)	**Linearity Constant** (-)	**Angle of Inflection** (deg)
752	T12-L2	3300	1.21	12.78	0.09	10
	L3-L5	4500	1.43	9.91	0.144	14
864	T12-L2	3300	0.75	4.26	0.18	10
	L3-L5	4500	2.62	NA	NA	NA
938	T12-L2	3300	1.52	11.27	0.13	9
	L3-L5	3300	2.04	7.54	0.27	11
939	T12-L2	2200	0.61	NA	NA	NA
	L3-L5	2200	0.13	3.65	0.04	18

942	T12-L2	3300	0.75	6.52	0.12	20
	L3-L5	4500	0.92	5.86	0.16	16
948	T12-L2	3300	1.00	7.34	0.14	15
	L3-L5	3300	1.72	7.79	0.22	24
949	T12-L2	3300	0.93	9.85	0.09	14
	L3-L5	4500	1.12	13.38	0.08	25
950	T12-L2	4500	0.05	6.52	0.01	6
953	T12-L2	2200	0.53	8.80	0.06	6
964	L3-L5	3300	0.08	6.82	0.01	15
965	T12-L2	4500	0.00013	4.20	3.1e-5	9
	L3-L5	3300	0.54	11.47	0.05	23
966	L3-L5	3300	1.33	6.15	0.22	19
968	T12-L2	3300	-0.20	2.22	-0.09	6
	L3-L5	3300	1.43	3.39	.042	12
969	T12-L2	2200	0.52	9.95	0.05	10
	L3-L5	4500	1.77	6.44	0.27	24
971	T12-L2	4500	0.89	7.64	0.12	16
	L3-L5	2200	0.68	8.74	0.08	16
972	T12-L2	4500	0.31	12.9	0.02	8
	L3-L5	3300	0.82	8.46	0.10	24
979	L3-L5	4500	2.30	NA	NA	NA
983	T12-L2	2200	1.82	6.86	0.27	10
	L3-L5	2200	0.78	6.03	0.13	10
985	T12-L2	4500	1.40	23.79	0.06	15
986	T12-L2	4500	0.54	8.88	0.06	17
	L3-L5	3300	0.74	12.72	0.06	20

TABLE C5

CALCULATED STIFFNESS VALUES FOR THE SIMULATION INJURY TESTS (NM/DEG)

	2200 N	**3300 N**	**4500 N**
Occupant T12-L2	2.65	2.66	2.70
Occupant L3-L5	2.75	2.61	2.50
Pedestrian T12-L2	2.63	2.95	2.62
Pedestrian L3-L5	2.46	2.53	2.50

Appendix D: GHBMC ligament definitions and geometry

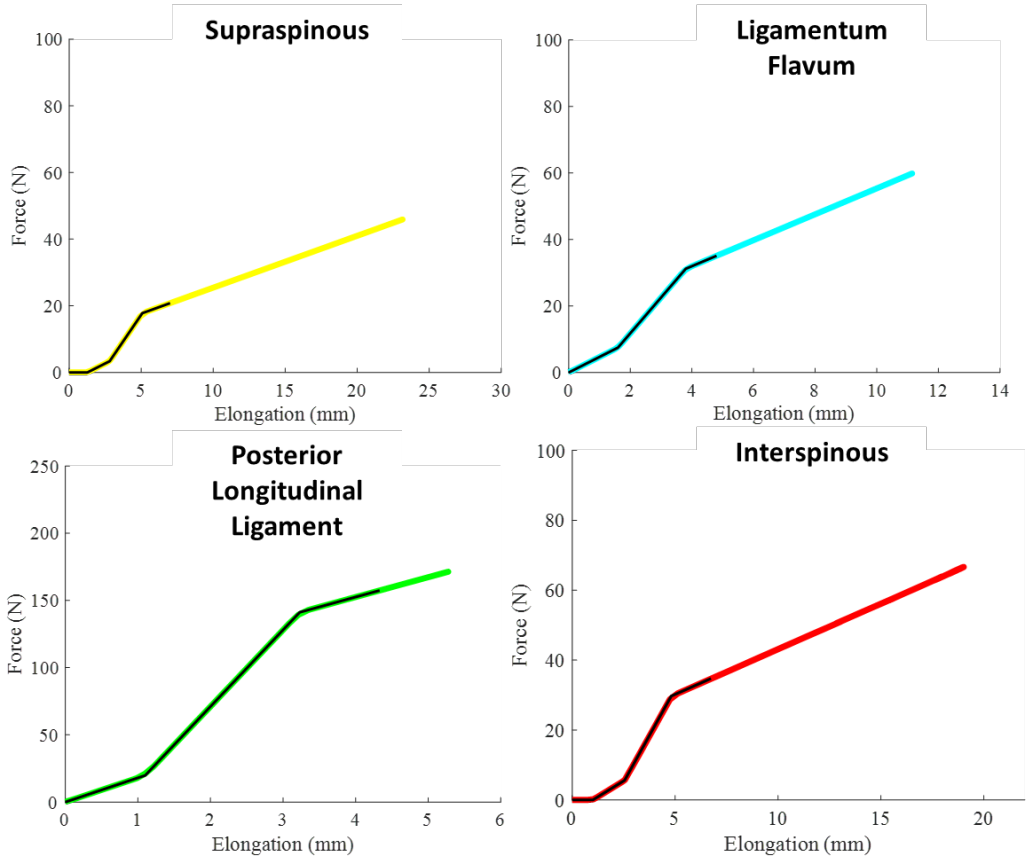

Fig. D1. Original ligament definition curves for the GHBMC (black) (permission granted from the GHBMC to include curves in the paper), along with the actual response curves for the supraspinous (yellow), ligamentum flavum (blue), posterior longitudinal ligament (green), and interspinous (red) force and elongation resulting from the injury test simulation with 3300 N axial compression. The curves depict responses of one fiber bundle (i.e. one beam element) of each of the four ligaments between the L4-L5 level. The actual response of the ligaments in this simulation extends past the ligaments' original definition.

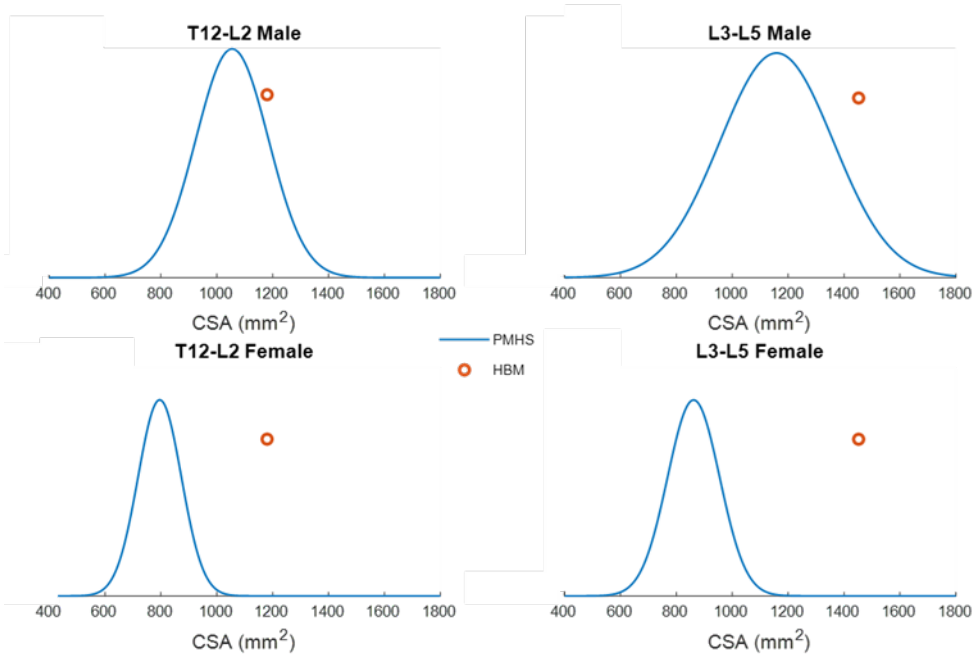

Fig. D2. Comparison of middle vertebrae superior endplate CSA for the PMHS and GHBMC HBM used in the study.